Assessment of tidal current energy in the Minas Passage, Bay of Fundy

R H Karsten*, **J M McMillan, M J Lickley,** and **R D Haynes**
Department of Mathematics and Statistics, Acadia University, Wolfville, Nova Scotia, Canada

The manuscript was received on 16 November 2007 and was accepted after revision for publication on 17 March 2008.

DOI: 10.1243/09576509JPE555

Abstract: The tidal power available for electricity generation from in-stream turbines placed in the Minas Passage of the Bay of Fundy is examined. A previously derived theory is adapted to model the effect of turbine drag on the flow through the Minas Passage and the tidal amplitude in the Minas Basin. The theoretical maximum power production over a tidal cycle is determined by the product of the amplitude of the forcing tide in the Bay of Fundy and the undisturbed volumetric flowrate through the Minas Passage. Although the extraction of the maximum power will reduce the flowrate through the Minas Passage and the tides in the Minas Basin by over 30 per cent, a significant portion of the maximum power can be extracted with little change in tidal amplitude as the initial power generation causes only an increase in the phase lag of the basin tides. Two-dimensional, finite-element, numerical simulations of the Bay of Fundy–Gulf of Maine system agree remarkably well with the theory. The simulations suggest that a maximum of 7 GW of power can be extracted by turbines. They also show that any power extraction in the Minas Passage pushes the Bay of Fundy–Gulf of Maine system closer to resonance with the forcing tides, resulting in increased tidal amplitudes throughout the Gulf of Maine. Although extracting the maximum power produces significant changes, 2.5 GW of power can be extracted with a maximum 5 per cent change in the tidal amplitude at any location. Finally, the simulations suggest that a single turbine fence across the Minas Passage can extract the same power as turbines throughout the passage but that partial turbine fences are less efficient.

Keywords: tidal power, alternative energy, renewable energy, energy assessment

1 INTRODUCTION

The Bay of Fundy harbours some of the world's highest tides, reaching over 6 m in amplitude in the Minas Basin (Figs 1 and 2). It has been shown [**1**, **2**] that the natural period of the Bay of Fundy–Gulf of Maine system is slightly larger than the 12.42 h period of the dominant semi-diurnal lunar tide – the M_2 tide. The resulting near-resonance is responsible for driving the high tides. The tides are a large source of energy; Greenberg [2] estimates a mean potential energy of 1.15×10^{14} J for the Minas Basin. For a tidal barrage, the potential power associated with this energy, estimated as twice the mean potential energy released over half a tidal period, is over 10 GW, about 15 per cent of Canada's current annual electrical power consumption [**3**]. This has encouraged the discussion of tidal power in the region for nearly 100 years.

Until recently, methods of harvesting tidal energy concentrated on capturing water in a dam or barrage at high tide and generating electricity by releasing the water at low tide. Although such constructions will obviously have a large impact on the local environment [**4**], previous research suggests that adding a barrier near the Minas Passage would also cause large changes throughout the entire Bay of Fundy–Gulf of Maine system as the system is pushed closer to resonance. As such, adding a barrier increases the amplitude of tides by 20 to 30 per cent along the coast of Maine and Massachusetts [**2**, **5**].

With the development of new in-stream tidal turbines, the prospect of tidal power in the Bay of Fundy is being revisited. As discussed in a variety of articles

**Corresponding author: Department of Mathematics and Statistics, Acadia University, Wolfville, Nova Scotia, Canada B4P 2R6. email: rkarsten@acadiau.ca*

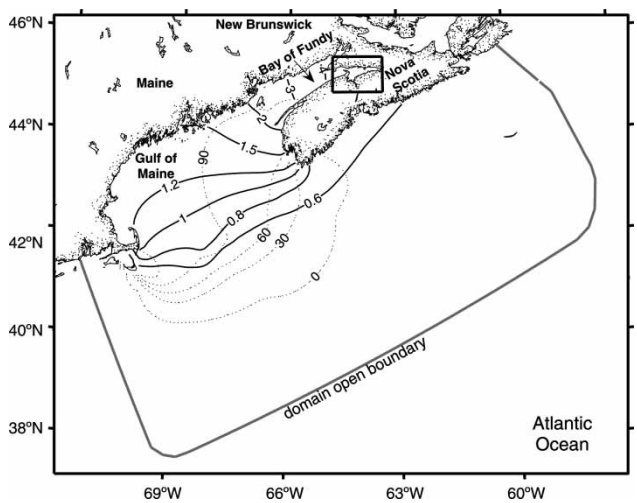

Fig. 1 The Bay of Fundy and Gulf of Maine region. The solid and dashed contours are the amplitude (m) and phase (°), respectively, of the simulated M_2 tide. The rectangle indicates the Minas Basin region shown in Fig. 2. The grey line is the open-ocean boundary of the computational domain

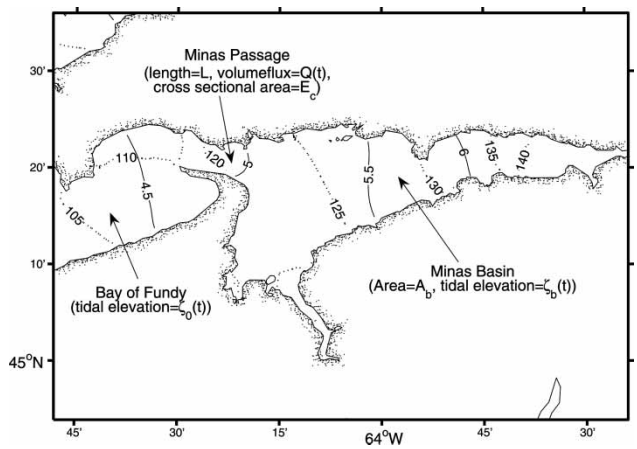

Fig. 2 The Minas Passage and the Minas Basin regions. The solid and dashed contours are the amplitude (m) and phase (°), respectively, of the simulated M_2 tide. The notation is that used in the model of the tides in section 2

[**3**, **4**, **6**–**9**], tidal turbines, which act much like wind turbines, are thought to offer many advantages over other forms of power generation. The high density of water and the predictability of the tides suggest that tidal turbines should be able to produce a large amount of reliable power, while the flexibility of individual turbines should make turbines more economically and ecologically attractive than tidal barrages. However, these advantages have yet to be established in practice as most operating turbine projects are small in scale [**4**, **9**].

Harnessing in-stream tidal power requires placing turbines in regions of high tidal flow. The strongest flow in the Bay of Fundy region occurs through the Minas Passage, the relatively deep, thin channel that connects the Minas Basin to the Bay of Fundy (Figs 1 and 2). The volumetric flowrate through the passage reaches roughly $10^6\,\mathrm{m^3/s}$ and sustains time-averaged, depth-averaged tidal currents of up to 3.28 m/s [**3**]. Recent surveys of potential tidal power sites have estimated the theoretical mean power of a flow through a channel, using a formula based on the kinetic energy flux in the undisturbed state [**3**, **7**]

$$P_{\mathrm{KE}} = E\left(\frac{1}{2}\rho\widehat{u^3}\right) \tag{1}$$

where ρ is the density of water, E the cross-sectional area of the channel and u the depth-averaged, upstream current speed. The term in brackets in equation (1) is the mean power density and is calculated by averaging u across the channel and over a tidal cycle. In reference [**3**], a mean power density of $6.036\,\mathrm{kW/m^2}$ and a passage cross-sectional area of $2.74 \times 10^5\,\mathrm{m^2}$ were used to give a power estimate of 1.9 GW for the Minas Passage, significantly less than the 10 GW estimate based on the mean potential energy.

Several aspects of this kinetic energy flux estimate require comment. First, an important aspect of the estimate is that the speed is cubed, so the power estimate increases rapidly with small increases in flow speed. Thus, formula (1) suggests that the best region for power is the narrowest portion of a channel with the highest flow speed. Second, the estimate contains no information about what forces the flow. This is extremely important for tidal flows. Extracting power and thus slowing the flow through the channel can increase the tidal head, the difference in tidal elevation across the channel. Thus, extracting power actually increases the forcing that drives the flow. Formulas that do not take this into account may underestimate the potential power.

Recently, Garrett and Cummins [**10**, **11**] have examined the potential of in-stream power generation from tidal flow in a channel. They reached two important conclusions: first, 'the average power produced need not be much less than in a conventional scheme with a dam', and second, 'there is no simple relationship … between the maximum average power and the average kinetic energy flux in the undisturbed state' [**10**]. Garrett and Cummins [**10**] derived an alternative formula for the maximum mean power that could be extracted for a channel between two large basins, given by

$$P_{\mathrm{avg}} = \gamma\rho g a Q_0 \tag{2}$$

where a is the amplitude of the tidal head across the channel, g the acceleration due to gravity, and Q_0 the maximum volumetric flowrate through the channel in the undisturbed state; γ is determined by the phase lag of the current behind the maximum elevation [**4**] and only varies over the small range between 0.20 and 0.24. In contrast to equation (1), this formula includes the tidal forcing through a and depends linearly on the current speed through the flowrate, Q_0. As well as the power depends on the volumetric flowrate, the formula does not differentiate between thin channels with strong flow and wide channels with weaker flow. It was shown in reference [**4**] that formula (2) agreed well with numerical simulations of tidal flow through channels east of Vancouver Island.

In considering the generation of power in the Minas Passage, it is important to examine the resulting reduction in flowrate through the passage. Any change in the flowrate will have a direct impact on the tides in the Minas Basin and, as discussed above, indirect effects throughout the Bay of Fundy and Gulf of Maine. Estimates of the reduction in flowrate vary. Bryden *et al.* [**8**, **12**] suggest that extracting 10–25 per cent of the kinetic energy flux in a channel flow would result in a 3–7 per cent change in the flowrate. In contrast, in the simulations of reference [**4**], the flowrate was reduced by 42 per cent when the maximum power was extracted, but by only 10 per cent when 44 per cent of the maximum power was extracted. These results were in agreement with the theory of Garrett and Cummins [**10**]. The different estimates of the available power and the resulting reduction in the flow lead to a large range of estimates for the realizable power available from the Minas Passage and suggest that further research is required.

This article addresses this need by assessing the resource potential of the Minas Passage. In section 2, algebraic formulas based on the theories of Garrett and Cummins [**10**, **11**] are used to estimate the power available and the resulting reduction in the basin tides as function of the turbine drag. In section 3, it is shown that the theory and, in particular, formula (2) are applicable to the Minas Passage *but only if* the parameter a is taken to be the amplitude of the forcing tides. In section 4, the theory is compared with numerical simulations of the Bay of Fundy–Gulf of Maine system using the finite-volume coastal ocean model (FVCOM) with turbines represented by increased bottom friction in the Minas Passage. After it is established that the theoretical estimates are accurate, the simulations are used to examine the effects that adding in-stream turbines to the Minas Passage would have on the tides throughout the Bay of Fundy and the Gulf of Maine. This is followed by a brief examination of how the location of turbines in the Minas Passage would affect the power generated. And in section 5, further discussion and conclusions are presented.

2 TIDAL STREAM MODEL

Recently, two theoretical models that calculated the potential power generated from tidal flow in a channel were derived by Garrett and Cummins. In reference [**10**], they examined the flow through a channel between two large bodies of water with a constant-amplitude tidal head. In reference [**11**], they examined a channel connecting a small basin to the open ocean. The critical difference between these two is that in reference [**10**] they assumed the tide in the basin was influenced by the flowrate through the channel, whereas in reference [**11**] they included the effects of flow acceleration. In a follow-up work, Blanchfield *et al.* [**13**] showed that the two models could be combined to examine the channel–small basin scenario and generalized formula (2) by defining a to be the amplitude of the open-ocean forcing tides and increasing the range of γ to 0.19–0.26.

Following reference [**13**], consider the dynamics of a channel connecting a small basin to the open ocean. Here, the Minas Passage connects the Minas Basin to the Bay of Fundy, as shown in Fig. 2. The channel has a variable cross-sectional area $E(x)$ and length L, whereas the basin has a surface area A_b. As discussed in detail in reference [**13**], the dynamics of the flow through the channel can be modelled by the equations

$$c\frac{dQ}{dt} + \lambda|Q|Q = g\,(\zeta_o - \zeta_b) \tag{3}$$

$$Q = A_b\frac{d\zeta_b}{dt} \tag{4}$$

where Q is the volumetric flowrate through the channel, ζ_o and ζ_b the tidal elevations in the ocean and the basin, respectively, λ the drag parameter, and

$$c = \int_0^L \frac{dx}{E(x)} \tag{5}$$

with x measured along the channel. The equations are derived from the momentum balance and continuity. Equation (3) states that the pressure force created by the difference in tidal elevations is balanced by the combination of the acceleration of flow through the channel and the non-linear drag in the channel. Here, the non-linear drag represents not only the drag associated with bottom friction and the addition of turbines but also all other non-linearities in the model, including non-linear advection and the non-linearities involved with the changes in domain as the tides rise and fall. Equation (4) is simply the conservation of volume: the change in volume of water in the basin as the surface elevation changes must equal the volume flowrate through the channel.

Blanchfield *et al.* [**13**] have solved the dynamical system given by equations (3) and (4) for both linear

and quadratic drag. For linear drag, the system can be solved analytically. This solution has the advantage of being easily used and interpreted but suffers because linear drag is not as realistic a model for bottom drag or turbine drag. For quadratic drag, the system must be solved numerically, and a graphical description of how the solutions depend on parameters is given in reference [**13**]. However, as discussed in section 3, the Minas Passage pushes the limits of this theory. As such, the parameter values that describe the Minas Passage are not included in the parameter range that Blanchfield *et al.* examined in reference [**13**]. Here, an approximate analytic solution for the quadratic drag system (3) and (4) is presented. It has the advantage of not requiring numerical solution while still being an accurate model for the flow in the Minas Passage in the undisturbed state and as turbines are added. A complete discussion of this approximate solution, including justification for the solution and an examination of its accuracy, is given in Appendix 2.

As in reference [**13**], the tidal elevation outside the channel in the open ocean is assumed to be a single sinusoid given by

$$\zeta_{\mathrm{o}} = a\cos(\omega t) \tag{6}$$

where a and ω are the known amplitude and frequency of the dominant tidal constituent, respectively. An approximate solution to equations (3) and (4) is given by assuming the basin tides are a single sinusoidal function given by

$$\zeta_{\mathrm{b}} = a_{\mathrm{b}}\cos(\omega t - \phi) \tag{7}$$

where a_{b} and ϕ are the unknown amplitude and phase lag of the basin tides, respectively. From equation (4), it follows that

$$Q = -A_{\mathrm{b}}\omega a_{\mathrm{b}}\sin(\omega t - \phi) \tag{8}$$

As shown in Appendix 2, it follows from equation (3) that the amplitude ratio, $R = a_{\mathrm{b}}/a$, and phase lag satisfy

$$R^2 = \frac{2\beta^2}{(\beta-1)^2 + \sqrt{(\beta-1)^4 + 4(\lambda^*)^2}} \quad \text{and}$$

$$\sin\phi = \frac{\lambda^*}{\beta^2}R^2 \tag{9}$$

where

$$\beta = \frac{g}{A_{\mathrm{b}}\omega^2 c}, \quad \lambda^* = \frac{8}{3\pi}\frac{ga}{(c\omega)^2}\lambda \tag{10}$$

The non-dimensional parameter β is determined by the geometry of the channel and basin and is independent of the drag [**13**]. It is also the ratio of the mean potential energy in the basin to the mean kinetic energy in the channel. And, as noted in reference [**13**], it is the ratio of the Helmholtz frequency of the basin to the frequency of forcing tides, with $\beta = 1$ being a special resonant case. In contrast, the parameter λ^* in equation (10) is the non-dimensional drag parameter in reference [**13**] multiplied by the factor $8/(3\pi)$ that arises in the derivation of the approximate solution (Appendix 2).

Given the approximate solution to the model, it is possible to examine the power generated by turbines. The non-linear drag force can be separated into two parts: that associated with the natural drag in the undisturbed channel and that associated with turbines added to the channel. As in reference [**13**], the drag parameter is written as

$$\lambda = \lambda_0 + \lambda_1 \tag{11}$$

where from now on the subscript 0 will be associated with the undisturbed state and the subscript 1 with the added turbines. The corresponding non-dimensional drag parameters are defined by equation (10).

The undisturbed state has amplitude ratio R_0 and phase ϕ_0 determined by equation (9) when $\lambda^* = \lambda_0^*$. Alternatively, these equations can be rearranged to give

$$\beta = \frac{R_0}{R_0 - \cos\phi_0}, \quad \lambda_0^* = \frac{\sin\phi_0}{(R_0 - \cos\phi_0)^2} \tag{12}$$

so that the values of β and λ_0^* can be determined from the observed values of R_0 and ϕ_0 This is particularly useful for determining λ_0^* because there is no simple formula for it if it includes all non-linearities. As well, the undisturbed maximum flowrate, Q_0, is given by

$$Q_0 = R_0 a A_{\mathrm{b}}\omega \tag{13}$$

Once the undisturbed state is determined, equation (9) can be used to determine how the solution will change as the turbine drag is changed.

The mean turbine power, P_{avg}, is given by

$$P_{\mathrm{avg}} = \rho\lambda_1\overline{|Q|Q^2} \tag{14}$$

where the over-line represents the average over a tidal cycle. In reference [**13**], it was shown that it was useful to relate the mean turbine power to a reference power given by

$$P_{\mathrm{ref}} = \rho g a Q_0 \tag{15}$$

which is, essentially, the work done by the forcing tides in driving the undisturbed flow through the channel. The non-dimensional mean turbine power is then

given by

$$P^*_{\text{avg}} = \frac{P_{\text{avg}}}{P_{\text{ref}}} \tag{16}$$

Using the solution above, it follows that

$$P^*_{\text{avg}} = \frac{\lambda^*_1}{2R_0\beta^2}R^3$$
$$= \frac{2^{1/2}\lambda^*_1}{R_0\left[(\beta-1)^2 + \sqrt{(\beta-1)^4 + 4(\lambda^*_0+\lambda^*_1)^2}\right]^{3/2}} \tag{17}$$

This is zero when $\lambda^*_1 = 0$, increases for small λ^*_1 but eventually decreases to zero as λ^*_1 becomes large and the flowrate tends to zero. Hence, there must be a maximum mean turbine power, hereafter simply called the maximum power. Finding this maximum can be reduced to solving the cubic

$$(\lambda^*_{1\text{m}} + \lambda^*_0)(\lambda^*_{1\text{m}} - 2\lambda^*_0)^2 - (\beta-1)^4(2\lambda^*_{1\text{m}} - \lambda^*_0) = 0 \tag{18}$$

for $\lambda^*_{1\text{m}}$, the drag parameter that gives the maximum power. Given $\lambda^*_{1\text{m}}$, equation (9) can be used to determine the amplitude, R_m, and the phase, ϕ_m, at maximum power. Then equation (17) can be used to calculate the maximum power, $(P_{\text{avg}})_{\text{max}}$, and, as in reference [**13**], the ratio of the maximum power to reference power is given by

$$\gamma = \frac{(P_{\text{avg}})_{\text{max}}}{P_{\text{ref}}} = (P^*_{\text{avg}})_{\text{max}}$$

Before examining the solution, insight can be gained by examining the extreme limits of the natural drag. In the limit of weak natural drag, $\lambda^*_0 = 0$, which gives the undisturbed state $R_0 = \beta/(1-\beta)$ and $\phi_0 = 0$, it is easy to show that

$$\lambda^*_{1\text{m}} = \sqrt{2}(\beta-1)^2, \quad R_\text{m} = \frac{1}{\sqrt{2}}R_0, \quad \phi_\text{m} = 45^\circ,$$
$$\gamma = \frac{1}{4} \tag{19}$$

A maximum power, i.e. one-fourth the reference power, is achieved when the amplitude of the basin tides and the flowrate have been reduced by a factor of $\sqrt{2}$ and the phase lag has increased to 45°.

In contrast, the strong natural drag limit, $\lambda^*_0 \gg (\beta-1)^2$ where $R_0 \approx \beta/\sqrt{2\lambda^*_0}$ and $\phi_0 \approx 90^\circ$, gives

$$\lambda^*_{1\text{m}} \approx 2\lambda^*_0, \quad R_\text{m} \approx \frac{1}{\sqrt{3}}R_0, \quad \phi_\text{m} \approx 90^\circ,$$
$$\gamma \approx \frac{1}{3^{3/2}} \tag{20}$$

In this case, the maximum power is a smaller fraction of P_{ref} because some power is dissipated by the natural drag and all the power is produced by a reduction in R, as the phase lag does not increase beyond 90°.

For all values of λ^*_0 and β, it follows that

$$\frac{1}{3^{3/2}} \leqslant \gamma \leqslant \frac{1}{4} \quad \text{and} \quad \frac{1}{\sqrt{3}} \leqslant \frac{R_\text{m}}{R_0} \leqslant \frac{1}{\sqrt{2}} \tag{21}$$

i.e. the maximum power is between 19 and 25 per cent of the reference power, and at the maximum power, the amplitude of the basin tide and channel flow is reduced to between 58 and 71 per cent of the undisturbed state. Note that the bounds (21) are almost identical to those found in reference [**13**] using the full solution. For example, equation (21) corresponds to $0.1925 < \gamma < 0.25$, whereas Blanchfield *et al.* [**13**] found that $0.19 < \gamma < 0.26$.

It is important to recognize that despite the small variation in γ, the maximum power always decreases significantly with increasing λ^*_0 as Q_0, and hence the reference power, is reduced by increased drag. Therefore, the power available is reduced by the natural drag in the undisturbed system.

The complete characteristics of the maximum-power solution versus λ^*_0 for three values of β are shown in Fig. 3. The values of β are chosen to give a range that includes the value for the Minas Passage but is not examined in reference [**13**]. The amplitude ratio of the undisturbed state, shown in plot (a), decreases like $1/\sqrt{\lambda^*_0}$ as the natural drag increases but this decrease occurs at higher values of λ^*_0 as β increases. The necessary turbine drag for maximum power, shown in plot (b), increases almost linearly with λ^*_0 and it increases significantly with increasing β.

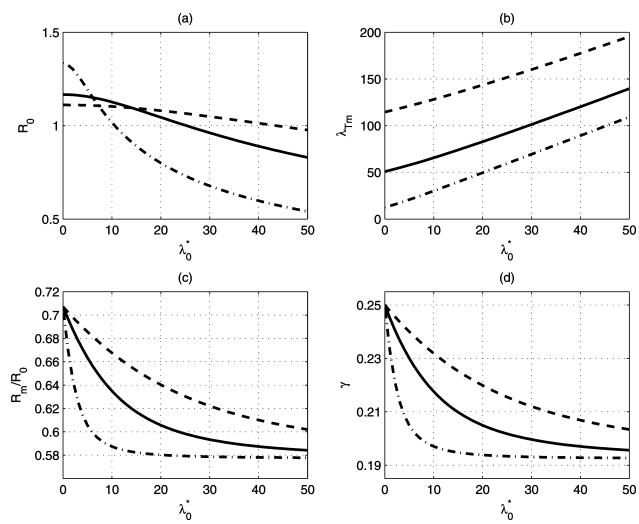

Fig. 3 Values of the (a) undisturbed amplitude ratio, (b) turbine drag, (c) amplitude ratio, and (d) turbine power at maximum turbine power versus the natural drag, λ^*_0. In each graph, curves are plotted for $\beta = 3, 7, 10$ as the dash-dot, solid, and dashed lines, respectively

The values for the amplitude and turbine power ratios shown in plots (c) and (d) start at the $\lambda_0^* = 0$ values in equation (19) and monotonically decrease to the large natural drag limit in equation (20), with the rate of decrease being smaller for larger β. As noted above, the values are restricted to the fairly strict bounds given in equation (21), and so these values are not particularly sensitive to the parameters β and λ_0^*. However, plot (b) does show that the turbine drag necessary for maximum power is sensitive to changes in β and λ_0^*.

A 30–40 per cent reduction in the Minas Basin tides would have a significant environmental impact. Therefore, it is reasonable to determine how much power can be extracted for a given acceptable change in tides. To do so, the power is rewritten as

$$P^*_{\text{avg}} = \frac{1}{2}(1 - \Delta\zeta_{\text{b}}) \left[\sqrt{1 - \cos^2\phi_0(1 - \Delta\zeta_{\text{b}})^2} - \sin\phi_0(1 - \Delta\zeta_{\text{b}})^2 \right] \tag{22}$$

where

$$\Delta\zeta_{\text{b}} = \frac{R_0 - R}{R_0} \tag{23}$$

is the relative change of the tidal amplitude in the Minas Basin and, also, of the flowrate in the Minas Passage. For small changes to the undisturbed system, $\Delta\zeta_{\text{b}} \sim 0$, it follows that

$$P^*_{\text{avg}} \approx R_0 \frac{\sin^2\phi_0 + 1}{2\sin\phi_0} \Delta\zeta_{\text{b}} \tag{24}$$

Significantly, this linear approximation has a very large slope for small ϕ_0 when $\sin\phi_0 \to 0$, i.e. a large proportion of the maximum turbine power can be obtained for a very small change in the amplitude of the basin tides if the phase lag in the undisturbed system is small.

3 APPLICATION TO THE MINAS PASSAGE

Before the theory is used to predict the tidal power available in the Minas Passage, the assumptions made in the derivation of equations (3) and (4) as presented in reference [**13**] need to be examined. The assumption that the forcing tides can be represented as a single sinusoidal function (6) is reasonable for the Bay of Fundy, where the M_2 tides dominate the tidal signal [**14**]. Therefore, in what follows, the frequency of the forcing and basin tides is that of the M_2 tides, i.e. $\omega = 2\pi/12.42$ per hour. However, it is also assumed that the forcing and basin tides rise and fall uniformly. As seen in Fig. 2, the tides in the Minas Basin vary in amplitude by about 25 per cent and in phase by over 15°, whereas the tides to the west of the Minas Passage vary by 10 per cent and 10°. However, if ζ_{o} and ζ_{b} represent appropriately averaged tides (see below), this variation does not appear to limit the usefulness of the theory. It is also assumed that the forcing tides are unaffected by the addition of turbines. As shown below, the tides in the Bay of Fundy to the west of the Minas Passage do decrease significantly in amplitude as turbines are added, and this does limit the accuracy of the model when the turbine drag is large. As well, it is assumed that E and A_{b} are constant in time and that the flowrate, Q, does not change along the channel. In fact, these vary 5–20 per cent due to the large tides, with the largest change seen in the cross-sectional area of the channel. However, the errors in making these assumptions are proportional to the square of the flowrate and so can reasonably be absorbed into the non-linear drag term in equation (3).

Similarly, the non-linear advection term has been absorbed into the non-linear drag term. It should be stressed that the flow is highly non-linear, as the velocities are on the order of several metres per second, and in the local momentum balance, the non-linear advection terms are very important. However, when averaged and integrated along the channel, the non-linear advection reduces in importance. In references [**10**, **11**, **13**], it is argued that this term will be dominated by flow separation as the flow exits the channel and therefore can be represented as a quadratic drag. The simulations discussed here do not provide direct evidence that the non-linear advection in the Minas Passage has the form of a non-linear drag. Instead they show stronger non-linear advection at the western entrance of the passage for both ebb and flood tide. This suggests that the geometry of the Minas Passage, most notably around Cape Split, plays an important role in the dynamics. The simulations do suggest that the channel-averaged non-linear advection is much weaker than the bottom-friction drag, and so the assumption that the dominant non-linear terms may be represented as a drag may be acceptable. Similarly, the effects of Coriolis forces and horizontal diffusion are also ignored as they are weak in all simulations.

In order to examine how well equation (3) captures the dynamics of the Minas Passage, each term in the equation is calculated using the data from a numerical simulation of the undisturbed tides. In Fig. 4, the results are plotted for one tidal period. For these calculations the direction of x was chosen to be eastward and the channel cross-sections are north–south cross-sections of the Minas Passage (Fig. 2). These directions were chosen for simplicity and consistency with the turbine simulations. The forcing-tide elevation, ζ_{o}, is calculated as the average tidal elevation along the western entrance to the Minas Passage. The basin-tide elevation, ζ_{b}, is calculated as the total water volume variation of the Minas Basin divided by A_{b}. And, the zonal flowrate, Q, is calculated at the eastern end of

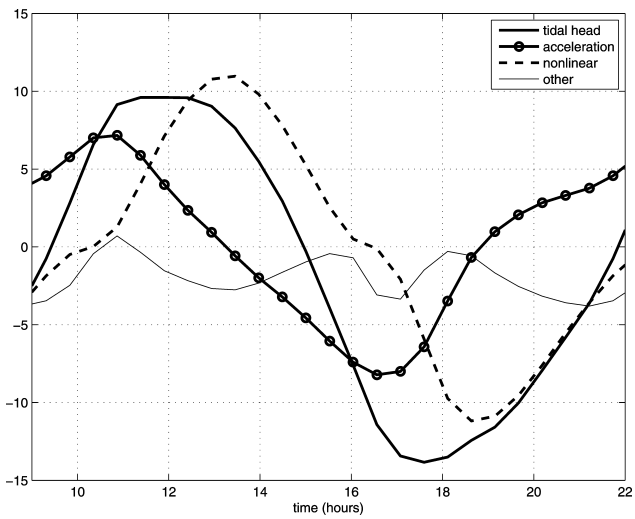

Fig. 4 The terms in the momentum balance (3) for the Minas Passage over a tidal period. The acceleration (solid line with circles) and non-linear drag (dashed) play an equally important role in balancing the pressure force (thick solid line). The imbalance between these three terms is shown by the thin black line

the Minas Passage. These last two definitions are chosen so that equation (4) must hold. The tidal head is the difference of the tidal elevations multiplied by g. The acceleration and non-linear drag are calculated using the flowrate, and parameters c and λ chosen to give the best least-squares fit to the tidal head. The imbalance of these terms represents the portion of the response to the tidal forcing that cannot be represented by the sum of a linear acceleration term and a quadratic drag, for example, the quadratic non-linearity of the form Q^2 that can be associated with non-linear advection. As the imbalance is small, it follows that equation (3) does capture the leading-order dynamics of the Minas Passage (see Appendix 2 for further discussion).

There are several other aspects of Fig. 4 worth noting. The pressure associated with the tidal head is initially balanced by an acceleration of the flow in the channel. As the flowrate increases, the drag becomes more important and plays the leading role in balancing the forcing. The high drag then leads to a de-acceleration of the flow even though the tidal head remains large. Note that the flow, which has the same phase as the drag term shown in Fig. 4, lags the tidal head by about 2 h. It should also be noted that the flow through the passage during flood and ebb tides is not as symmetric as the figure suggests. During the flood tide, the local velocities reach higher values, resulting in greater frictional dissipation and higher non-linear advection. Conversely, during ebb tide, stronger meridional flow results in a stronger Coriolis force. Finally, as turbines are added and the drag increases, the balance (3) becomes more accurate, with a leading-order balance between the pressure and the non-linear drag while the acceleration and all other terms decrease in importance.

The best-fit values of the parameters used to produce Fig. 4 are

$$c_{\text{fit}} = 6.19 \times 10^{-2}\,\text{m}^{-1} \quad \lambda_{\text{fit}} = 1.89 \times 10^{-11}\,\text{m}^{-4} \tag{25}$$

These values of c and λ can be compared with the values given by equation (5) and the formula for the bottom-friction drag given by [**13**]

$$\lambda = \int_0^L \frac{\kappa_0}{h(x)E(x)^2}\,\mathrm{d}x \tag{26}$$

where $\kappa_0 = 0.0026$ is the bottom-drag coefficient used in the numerical simulations and $h(x)$ the cross-channel average depth of the Minas Passage. These formulas give $c = 3.78 \times 10^{-2}\,\text{m}^{-1}$ and $\lambda = 6.00 \times 10^{-12}\,\text{m}^{-4}$. The differences are significant. In particular, the fact that $\lambda_{\text{fit}} > 3\lambda$ indicates that quadratic non-linearities other than bottom friction are very important in the flow. This is not surprising given the strong flow and high tides. The large value of c_{fit} suggests that a significant portion of the pressure force across the Minas Passage acts on the non-uniform sides of the channel and does not accelerate the zonal flow. This is, in large part, a result of choosing x in the zonal direction and not in a more appropriate along-channel direction.

Parameter values for the Minas Basin and the Minas Passage are listed in Table 1. The values for a_{b} and a are taken to be the averaged undisturbed tidal amplitude in the Minas Basin and along the western entrance to the Minas Passage, respectively. The cross-sectional area corresponds to the average area of the Minas Passage, and the area of the Minas Basin is the area that is wet greater than 50 per cent of the time. Using

Table 1 Parameters and their values for the Minas Passage and the Minas Basin

Parameter	Description	Calculated value
ρ	Water density	$1026\,\text{kg/m}^3$
L	Length of the Minas Passage	1.2×10^4 m
E	Cross-sectional area of the Minas Passage	$3.1 \times 10^5\,\text{m}^2$
A_{b}	Surface area of the Minas Basin	$1.0 \times 10^9\,\text{m}^2$
ω	M_2 tidal frequency	$1.4 \times 10^{-4}\,\text{s}^{-1}$
a_{b}	Amplitude of basin tides	5.30 m
a	Amplitude of forcing tides	4.71 m
h	Average depth of the Minas Passage	53 m

these values, equations (13) and (15) give

$$Q_0 = 7.5 \times 10^5\,\mathrm{m^3/s} \quad P_{\mathrm{ref}} = 35\,\mathrm{GW} \tag{27}$$

Assuming that the non-linear term is completely due to bottom friction, equation (10) gives

$$\beta = 13.0 \quad \lambda_0^* = 9.84 \tag{28}$$

In contrast, the values of β and λ_0^* that correspond to the best-fit values of c and λ_0 given in equation (25) are

$$\beta = 7.91 \quad \lambda_0^* = 11.5 \tag{29}$$

Alternatively, equation (12) can be used to determine β and λ_0^*. The numerical simulations give

$$R_0 = 1.12 \quad \text{and} \quad \phi_0 = 12.4^\circ \tag{30}$$

These are comparable with the observations in Table 3 given in Appendix 3, where the amplitude ratio and phase lag between Diligent River to the west of the Minas Passage and Five Islands to the east are 1.11 and 12°, respectively. Using equation (12) with equation (30) gives

$$\beta = 7.62 \quad \lambda_0^* = 9.89 \tag{31}$$

The range of possible values for β and λ_0^* reflects the difficulty in precisely determining the best values for these parameters. Fortunately, the theory suggests that the turbine power is not particularly sensitive to the choice of β and λ_0^*, as shown in Fig. 3. Hereafter, the values given in equation (31) will be used as they are the easiest to calculate, they give the undisturbed state exactly, and they circumvent the issues of determining other parameters or fitting the model precisely.

4 NUMERICAL SIMULATIONS

The Bay of Fundy–Gulf of Maine tides are simulated using a two-dimensional, finite-volume model (FVCOM) to verify the theoretical estimates and examine far-field effects of extracting power. FVCOM was developed by Changsheng Chen and Geoffrey Cowles from the University of Massachusetts-Dartmouth, along with Robert C. Beardsley from Woods Hold Oceanographic Institution [**15**, **16**]. The model domain, shown in Fig. 1, extends far beyond the Bay of Fundy–Gulf of Maine system so that it can respond freely to the tidal forcing. The model was run by specifying the M_2 phase and amplitude at the open boundary. The resulting tidal amplitude and phase were then compared with observations. On average, the accuracy was within 8 cm in amplitude and 3.1° in phase, comparable with other studies [**2**, **5**, **14**]. Other aspects of the model tides, such as energy, dissipation rates, etc., were also compared with these studies to ensure that all aspects of the model were realistic. The details of the model and the comparison to observed tides are given in Appendix 3.

In order to compare the above theory to the results of simulations, it was necessary to model the effect that turbines would have on the tides. As in reference [**4**], the turbines were represented by increasing the bottom friction over the entire Minas Passage (Fig. 2). Such a scenario is a rough model of a turbine farm or a series of turbine fences across the Minas Passage. Following reference [**4**], the amount of power that was extracted by the turbines is calculated as a fraction of the total bottom-friction drag power, D, as follows

$$P_{\mathrm{avg}} = \frac{\kappa_1}{\kappa_1 + \kappa_0} D \tag{32}$$

where κ_1 is the drag coefficient associated with the turbines and κ_0 the bottom-friction drag coefficient. The value of λ_1 is calculated using equation (26) with κ_1.

A comparison of the results of the simulations and the theory is shown in Fig. 5. In Fig. 5(a), the theoretical amplitude ratio R is plotted versus λ_1^*. For the numerical simulations, both the ratio of the tidal amplitude in the basin to the constant amplitude scale a (o's) and the ratio of the basin tides to the changing amplitude of the tides at the entrance to the Minas Passage (x's) are plotted. It is clear that the theory captures

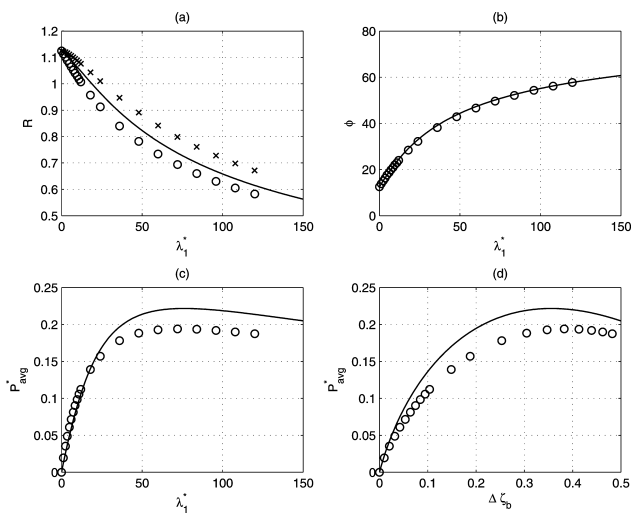

Fig. 5 (a) The ratio of the amplitude of the basin tides to the forcing tide, R, versus λ_1^*. (b) The phase lag of the basin tides, ϕ, versus λ_1^*. (c) The non-dimensional turbine power, P_{avg}^*, versus λ_1^*. (d) The non-dimensional turbine power, P_{avg}^*, versus the relative amplitude change in the basin, $\Delta\zeta_{\mathrm{b}}$. In each graph, the quadratic theory with β and λ_0^* given by equation (31) (solid line) and the numerical simulations (markers) are plotted

the decrease in the basin tides as the turbine drag is increased. However, as increasing the turbine drag also decreases the tides at the entrance of the Minas Passage, the ratio of the amplitudes does not decrease as quickly as R. This has important consequences for power generation. As the ratio decreases below one, it increases the tidal head, resulting in stronger flow and greater power. Therefore, the fact that the ratio decreases more slowly for the simulations will mean that the power generation in the simulations will be lower than that predicted by the theory for large λ_1^*.

In Fig. 5(b), the phase lag, ϕ, from the theory and simulations is plotted. It is clear that the theory captures how the phase lag depends on λ_1^*. It is the initial rapid increase in phase lag that maintains a strong tidal head even when the forcing and basin tides have the same amplitude.

In Fig. 5(c), the turbine power from the theory and simulations is plotted. For small λ_1^*, the two agree remarkably well. However, as λ_1^* increases, the difference in the tide amplitude ratios shown in Fig. 5(a) causes the power in the simulations to be lower than the theory predicts. The power initially increases rapidly to a maximum and then tails off slowly, as the theory predicts. The maximum power in the simulations of $0.194P_{\text{ref}}$ occurs at $\lambda_1^* = 71.9$ when the basin tides have been reduced by 36 per cent and the phase lag is 55°, whereas the theory predicts $P_{\text{m}} = 0.222P_{\text{ref}}$ at $\lambda_{1\text{m}}^* = 76.1$, where $\Delta\zeta_{\text{b}} = 0.36$ and $\phi_{\text{m}} = 51°$. Again, there is very good agreement although the maximum power is only 87 per cent of what the theory suggests. Using equation (27), the maximum power in the simulations corresponds to 6.95 GW. The turbine drag coefficient for maximum power is $\kappa_1 = 0.06$, over 20 times the bottom-friction drag coefficient.

Finally, in Fig. 5(d), the turbine power versus the relative change in the Minas Basin tides, $\Delta\zeta_{\text{b}}$, is plotted. As one would expect from the previous graphs, the theory and simulations agree almost exactly for small $\Delta\zeta_{\text{b}}$ but differ at larger values as the simulation turbine power is lower. The maximum power occurs when the basin tides are reduced by 36 per cent, but power levels of roughly 50 per cent the maximum power can be reached with only a 7.5 per cent reduction in the basin tides. As the simulations agree so well with theory for small $\Delta\zeta_{\text{b}}$, formula (24) is valid, giving

$$P_{\text{avg}} \approx 4.8\Delta\zeta_{\text{b}}P_{\text{ref}} \approx 77\Delta\zeta_{\text{b}}\,\text{GW} \tag{33}$$

Remarkably, for low levels of power extraction, 0.77 GW of turbine power can be extracted for each percentage reduction in the Minas Basin tides!

It is obvious that extracting power in the Minas Passage causes changes to the phase and amplitude of the tides in the Minas Basin. However, the extraction of power also causes changes throughout the Bay of Fundy and the Gulf of Maine. In Fig. 6, the *decrease* in tidal amplitude that occurs at maximum power extraction for the upper Bay of Fundy is plotted. As discussed above, the tides in the Minas Basin are reduced significantly, by over 2 m for most of the basin. The reduction in tides decreases rapidly west of the Minas Basin: the tides are reduced by 1–2 m in the Minas Passage and by 30–50 cm in the region to the west of Minas Passage. Over the rest of the upper Bay of Fundy, including the Chignecto Bay, the tidal amplitudes are reduced by less than 20 cm.

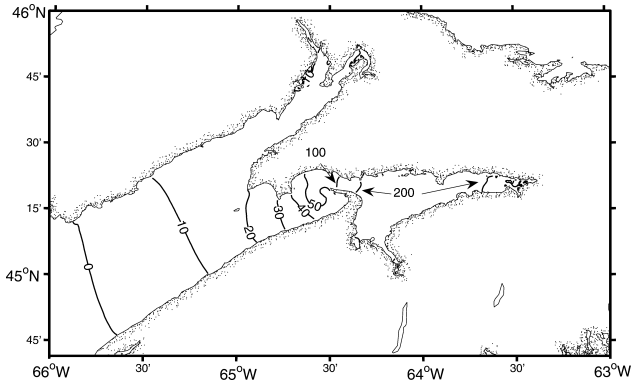

Fig. 6 The *decrease* in amplitude of the tides (cm) in the upper Bay of Fundy as a result of extracting the maximum amount of power from the Minas Passage

Conversely, tidal amplitudes are increased throughout the Gulf of Maine. In Fig. 7, the *increase* in tidal amplitude that occurs at maximum power extraction for the Gulf of Maine is plotted. The tides increase by over 12 cm for most of the gulf, with larger values to the west, reaching a maximum of nearly 25 cm in the

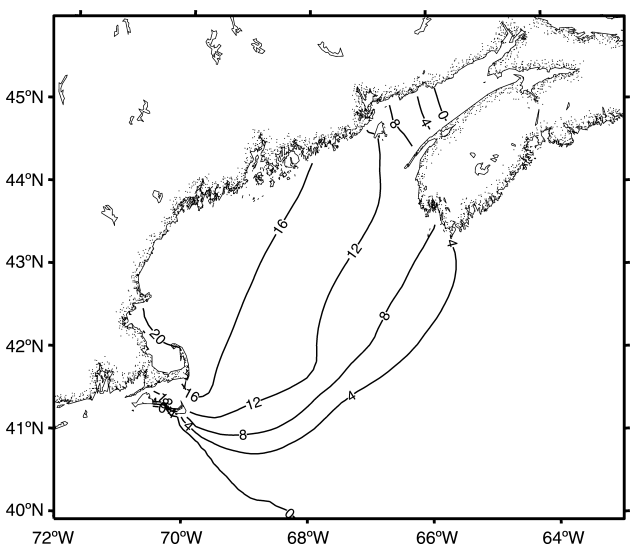

Fig. 7 The *increase* in amplitude of the tides (cm) in the Gulf of Maine as a result of extracting the maximum amount of power from the Minas Passage

Boston area. The tides also increase at the mouth of the Bay of Fundy by about 8 cm.

These results should be contrasted to simulations that place a barrier across the Minas Passage. A barrier across the Minas Passage produces large increases in the tides throughout the Bay of Fundy and the Gulf of Maine, with increases in the upper Bay of Fundy of about 30 cm and large increases in the Gulf of Maine of about 45 cm. In the other works [**2**, **5**], barriers and dams have produced similar large increases in the tides throughout the domain. Finally, Fig. 7 shows that although the entire Gulf of Maine is affected by turbines in the Minas Passage, tides in the regions outside the Gulf, for example, along the South Shore of Nova Scotia and in the deep ocean, show generally less than a 1 cm change in amplitude.

The changes in the tidal amplitudes can be related to the changes in the resonant period of the Bay of Fundy–Gulf of Maine system as turbines change the flow through the Minas Passage. The resonant period of the system was calculated as the period of the forcing tides that produced the maximum total energy in the system. Using this measure, the undisturbed system had a resonant period of 12.85 h, above the period of the M_2 tides of 12.42 h. As the turbine drag is increased, the resonant period of the system decreases. For weak turbines, $\kappa_1 = 0.005$, the resonant period is reduced to 12.80 h. For values near maximum turbine power, $\kappa_1 = 0.05$, the resonant period is reduced to 12.59 h, significantly closer to the forcing period, resulting in higher tides for most of the system. In comparison, for a barrier at the Minas Passage, the resonant period is 12.50 h, still closer to the resonant period and hence producing still greater tidal amplitudes.

In order to further examine the effects of extracting power, the relative change in amplitude versus the turbine power, P_{avg}, for a number of locations is plotted in Fig. 8. As noted before, extracting the maximum power can result in large changes in the tides (>30 per cent) in the Minas Passage and the Minas Basin and significant far-field changes (∼15 per cent). The far-field effects are still significantly smaller than those with a full barrier. However, the figure also illustrates that significant power can be extracted with limited effects on the tidal regime throughout the domain. For example, 4 GW of power can be extracted with less than a 10 per cent change in tidal amplitudes throughout the domain, and 2.5 GW can be extracted with less than a 5 per cent change. It should be noted that any power extraction will produce changes throughout the Bay of Fundy and Gulf of Maine, but the largest changes are always in the Minas Basin. Therefore, formula (33) can be used as an upper bound of the changes in tides throughout the system.

The theory suggests that the power extracted from a region is a function of the tidal forcing and the channel

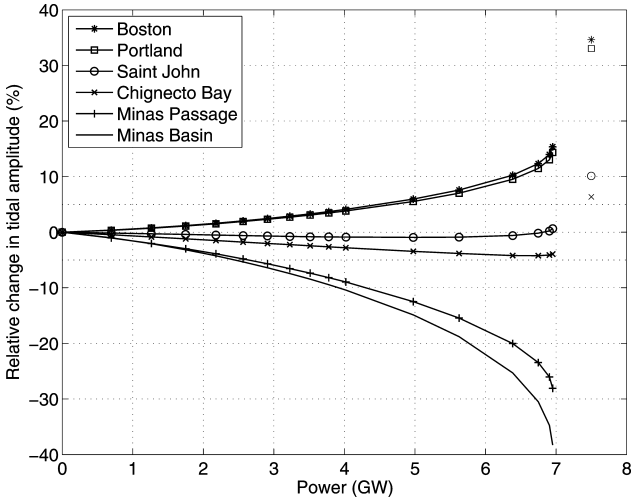

Fig. 8 The relative change in amplitude of the tides (%) versus extracted turbine power (GW). The markers to the right are the changes for the top four curves when a barrier is placed across the entrance to the Minas Passage. See Fig. 10 in Appendix 3 for the location of the stations

flowrate, not simply the local flow. The previous simulations had turbines throughout the Minas Passage. A more realistic scenario would be a single turbine fence across the passage. The theory suggests that the maximum power should be the same for such a thin fence. To test this, a series of simulations were run where turbines were only placed along one-fourth of the total length of the Minas Passage.

The theory also assumes that all the channel flow passes through the turbines, that is, the turbines are a fence extending across the channel. In a more realistic scenario, turbines will not be placed in shallow water and thus will not extend across the entire cross-section of the channel. This situation is examined in some detail in reference [**17**], where it was shown that the potential power is reduced by a factor of between one-third and two-third for a partial turbine fence as compared with a complete turbine fence because energy is lost as the turbine wake is dissipated. It was noted in reference [**4**] from preliminary numerical simulations that partial fences are ineffective 'as the water will tend to avoid it and flow through the unrestricted part of the cross-section.' Here, a simple case where turbines are only placed where the depth of the Minas Passage exceeds 60 m is considered.

In order to compare these runs to the original simulations, the value of κ_1 used in the definition of λ_1^* is adapted as follows

$$\kappa_1 = \frac{A_1}{A_{\text{MP}}}\kappa_{\text{A}}$$

where κ_{A} is the frictional coefficient associated with the turbines employed over area A_1 and A_{MP} the area

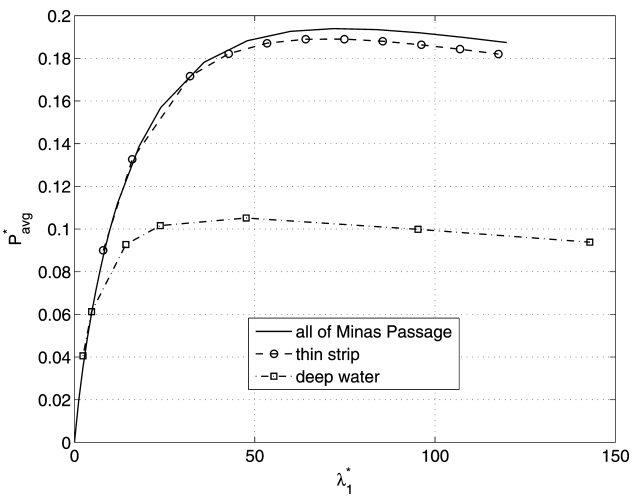

Fig. 9 The non-dimensional turbine power, P^*_{avg}, versus the non-dimensional turbine drag, λ^*_1, for numerical simulations where turbines were placed over the entire Minas Passage (solid line), only a thin strip of the Minas Passage (dashed with circles), and only the deep Minas Passage (dot-dash with squares)

of the Minas Passage. The definition suggests that to obtain the same net drag over a reduced turbine area, the drag coefficient of the turbines must be increased, that is, each turbine must work harder.

Figure 9 shows the comparison of the two scenarios to the original simulations. The thin strip of turbines gives virtually identical results to the original simulations, suggesting that a single turbine fence across the passage is sufficient to capture the maximum amount of power. Although the deep-turbines scenario gives similar results for small values of drag, the maximum power obtained is only about one-half of the original simulations. The explanation for this reduced power lies in the fact that as the turbine drag increases, the flow through the region without turbines increases. And, thus, an increasing fraction of the flow through the channel does not produce power.

These two scenarios offer a glimpse into how the theory and power estimates presented here might be extended to more realistic scenarios. A more detailed discussion of the theory of isolated turbines and partial fences is given in reference [**17**].

5 DISCUSSION AND CONCLUSION

Tidal power has recently received renewed attention as the search for renewable, green power sources intensifies. Recent publications [**4**, **10**, **11**, **13**] have established that in-stream turbines can generate significant power. Here, the high tides in the Bay of Fundy and, in particular, the large tidal flows through the Minas Passage are examined. A theoretical framework and the results of numerical simulations argue that up to 7 GW of power could be extracted from the Minas Passage. This is more than three times as large as the estimate in reference [**3**] based on the kinetic energy in the Minas Passage.

An adaptation of the theory of Garrett and Cummins [**10**, **11**, **13**] gives algebraic formulas that can be used to calculate the maximum turbine power and the change in local tides in response to the turbines. Despite many assumptions, the theory agrees remarkably well with the numerical simulations of the Bay of Fundy–Gulf of Maine system that represented turbines in the Minas Passage by an increase in the bottom drag. The biggest difference between the theory and the simulations is that the amplitude of the forcing tide in the Bay of Fundy decreases as the turbine drag increases, whereas the theory assumes it is constant. This reduces the tidal head at large values of the turbine drag and decreases the maximum power. As well, formula (2) with a given by the amplitude of the forcing tides is verified. This suggests that the greatest tidal power will be possible in channels where the product of the flowrate through the channel and the tidal amplitude at the entrance of the channel is large.

The effects of extracting the maximum power are significant. The tides in the Minas Passage and the Minas Basin would decrease by 36 per cent. The Bay of Fundy–Gulf of Maine system would be pushed closer to resonance with the M_2 tide, leading to an increase in tides of over 15 per cent along the northeast coast of the USA. However, a significant amount of power can be extracted with limited effects on both the local and far-field tides. For example, 2.5 GW of power can be extracted with at most a 5 per cent change in the tidal amplitudes. And, for small amounts of power extraction, 0.77 GW of power can be extracted for each percentage change in relative tidal amplitudes.

The simulations also indicate that the maximum rate of power extraction can be achieved with a single turbine fence and that partial turbine fences, while able to extract a significant portion of the maximum power, are less efficient.

It should be noted that in reference [**9**], Blanchfield *et al.* applied the theory of reference [**13**] to Masset Sound, a channel–basin system with a significantly different geometry than the Minas Passage–Basin system. In reference [**9**], the undisturbed state gives $\beta = 1.45$ and $\lambda^*_0 = 8$ and the system behaves like the strong natural drag limit discussed in section 2. Although the differences in systems are interesting. It is particularly worth noting that the inclusion of other tidal constituents can increase the maximum power significantly, by 9 per cent [**9**]. Initial calculations suggest that a similar increase in the maximum power may be possible for the Minas Passage. Numerical simulations that include the forcing of other tidal constituents

need to be run to test this possibility, but these simulations must necessarily be run for longer times to calculate an appropriate mean power.

As well, the resolution of the numerical simulations presented here may limit the ability to examine the non-linear aspects of the flow. In particular, the simulations do not show a strong effect of flow separation as the flow exits the channel, as discussed in reference [**10**, **11**, **13**]. Instead, the geometry of the channel plays a more important role by creating a strong, non-linear jet near Cape Split, especially during flood tide. The resolution is also not sufficient to examine the details of the turbulent flow past a partial fence or an isolated turbine as discussed in reference [**17**] and thus may not be sufficient to examine the effectiveness of turbines downstream of other turbines.

The results of Sucsy *et al.* [**5**] suggest that a three-dimensional model does not improve the accuracy of modelling the tides in the Bay of Fundy or significantly change the effects of including a barrier. However, a three-dimensional model would allow a more accurate representation of turbines that extract power from only a portion of the water column. It would also allow the power associated with turbines to be properly differentiated from that associated with bottom friction. Thus, the goal of the ongoing work is to extend the current results to the power potential of a farm of realistic, isolated turbines using a higher-resolution, three-dimensional model of the Minas Passage.

ACKNOWLEDGEMENTS

The authors thank David Greenberg for all his help with the numerical grid and observations. As well, the comments of two anonymous reviewers greatly improved the paper. The authors also thank the Natural Sciences and Engineering Research Council of Canada for its financial support. J. McMillan and M. Lickley were both supported by an NSERC USRA; R. Karsten and R. Haynes have both received NSERC Discovery Grants.

REFERENCES

1 **Garrett, C.** Tidal resonance in the Bay of Fundy and Gulf of Maine. *Nature*, 1972, **238**, 441–443.
2 **Greenberg, D. A.** A numerical model investigation of tidal phenomena in the Bay of Fundy and Gulf of Maine. *Mar. Geodesy*, 1979, **2**(2), 161–187.
3 **Triton Consultants Ltd.** Canada ocean energy atlas (phase 1) potential tidal current energy resources analysis background, 2006 available from http://homepage.mac.com/max.larson/Triton/download/TritonCanadaTidalPowerMay2006.pdf.
4 **Sutherland, G., Foreman, M.,** and **Garrett, C.** Tidal current energy assessment for Johnstone Strait, Vancouver Island. *Proc. IMechE, Part A: J. Power and Energy*, 2007, **221**(A2), 147–157.
5 **Sucsy, P. V., Pearce, B. R.,** and **Panchang, V. G.** Comparison of two- and three-dimensional model simulation of the effect of a tidal barrier on the Gulf of Maine tides. *J. Phys. Oceanogr.*, 2006, **23**(6), 1231–1248.
6 **Blunden, L. S.,** and **Bahaj, A. S.** Tidal energy resource assessment for tidal stream generators. *Proc. IMechE, Part A: J. Power and Energy*, 2007, **221**, 137–146.
7 **Hagerman, G., Fader, G., Carlin, G.,** and **Bedard, R.** EPRI Nova Scotia tidal in-stream energy conversion survey and characterization of potential project sites, December, 2006 available from http://oceanenergy.epri.com/attachments/streamenergy/reports/Tidal_003_NS_Site_Survey_Report_REV_2.pdf.
8 **Bryden, I. G., Grinstedb, T.,** and **Melville, G. T.** Assessing the potential of a simple tidal channel to deliver useful energy. *Appl. Ocean Res.*, 2004, **26**, 198–204.
9 **Blanchfield, J., Garrett, C., Rowe, A.,** and **Wild, P.** Tidal stream power resource assessment for Masset Sound, Haida Gwaii. *Proc. IMechE, Part A: J. Power and Energy*, 2008, in press.
10 **Garrett, C.** and **Cummins, P.** The power potential of tidal currents in channels. *Proc. R. Soc.*, 2005, **461**, 2563–2572.
11 **Garrett, C.** and **Cummins, P.** Generating power from tidal currents. *J. Waterway, Port Coast. Ocean*, 2004, **130**, 114–118.
12 **Bryden, I. G., Couch, S. J., Owen, A.,** and **Melville, G.** Tidal current resource assessment. *Proc. IMechE, Part A: J. Power and Energy*, 2007, **221**(A2), 125–135.
13 **Blanchfield, J., Garrett, C., Wild, P.,** and **Rowe, A.** The extractable power from a channel linking a bay to the open ocean. *Proc. IMechE, Part A: J. Power and Energy*, 2008, **222**(A3), 289–297.
14 **Dupont, F., Hannah, C.G.,** and **Greenberg, D.** Modelling the sea level of the upper Bay of Fundy. *Atmosphere-Ocean*, 2005, **43**, 33–47.
15 **Chen, C., Beardsley, R. C.,** and **Cowles, G.** An unstructured grid, finite-volume coastal ocean model (FVCOM) system. *Oceanography*, 2006, **19**(1), 78–89.
16 **Chen, C., Beardsley, R. C.,** and **Cowles, G.** *An unstructured grid, finite-volume coastal ocean model. FVCOM User Manual*, SMAST/UMASSD Technical Report-04-0601, p. 183, 2006.
17 **Garrett, C.,** and **Cummins, P.** The efficiency of a turbine in a tidal channel. *J. Fluid Mech.*, 2007, **588**, 243–251.

APPENDIX 1

Notation

a	amplitude of forcing tides (m)
A_b	surface area of the Minas Basin (m^2)
c	acceleration coefficient (m^{-1})
E	cross-sectional area of the Minas Passage (m^2)
g	acceleration due to gravity (m/s^2)
h	depth of the Minas Passage (m)
L	length of the Minas Passage (m)
P_{avg}	mean turbine power (GW)

Q	volumetric flowrate through the channel (m^3/s)
Q_0	maximum flowrate in the undisturbed state (m^3/s)
R	the ratio of the amplitude of the basin tides to the forcing tides
t	time (s)
u	velocity (m/s)
x	along-channel coordinate (m)
β	non-dimensional basin geometry parameter
γ	maximum power ratio
$\Delta\zeta_b$	the relative change in the basin tides
ζ	water surface elevation (m)
κ	bottom-drag coefficient
λ	drag parameter (m^{-4})
ρ	density of sea water (kg/m^3)
ϕ	phase lag of basin tides
ω	frequency of M_2 tides (s^{-1})

Superscripts

*	non-dimensional value
$\overline{Q}$	average of Q over a tidal period

Subscripts

0	associated with the undisturbed state
1	associated with turbines
b	associated with the basin
o	associated with the open-ocean forcing
m	at maximum turbine power
MP	associated with the Minas Passage
ref	reference values

APPENDIX 2

Derivation of an approximate theoretical solution

Consider the dynamical system given by equations (3) and (4) with the forcing tides given by equation (6), that is

$$c\frac{\mathrm{d}Q}{\mathrm{d}t} + \lambda|Q|Q = g\,(\zeta_o - \zeta_b) \tag{34}$$

$$Q = A_b\frac{\mathrm{d}\zeta_b}{\mathrm{d}t} \tag{35}$$

with

$$\zeta_o = a\cos(\omega t) \tag{36}$$

As the forcing tides are periodic, it is reasonable to assume the solution to equation (34) can be written as a Fourier series, which, using equation (35), can be written as

$$\zeta_b = \sum_{n=1}^{\infty}\alpha_n\cos(n\omega t - \phi_n) \quad \text{and}$$

$$Q = -\omega A_b\sum_{n=1}^{\infty}\alpha_n\sin(n\omega t - \phi_n) \tag{37}$$

Multiplying equation (34) by ρQ and averaging over a tidal cycle gives

$$c\rho\overline{Q\frac{\mathrm{d}Q}{\mathrm{d}t}} + \rho\lambda\overline{|Q|Q^2} = \rho g\left(\overline{Q\zeta_o} - \overline{Q\zeta_b}\right) \tag{38}$$

Here, the over-line represents the average of a quantity over a tidal cycle, that is

$$\overline{Q} = \frac{1}{T}\int_{t_0}^{T+t_0} Q\,\mathrm{d}t$$

Since ζ_b and Q are periodic, it follows that

$$\overline{Q\frac{\mathrm{d}Q}{\mathrm{d}t}} = \frac{1}{2}\overline{\frac{\mathrm{d}Q^2}{\mathrm{d}t}} = 0$$

and, using equation (35), that

$$\overline{Q\zeta_b} = A_b\overline{\frac{\mathrm{d}\zeta_b}{\mathrm{d}t}\zeta_b} = \frac{1}{2}A_b\overline{\frac{\mathrm{d}\zeta_b^2}{\mathrm{d}t}} = 0$$

And so, equation (38) reduces to

$$\rho\lambda\overline{|Q|Q^2} = g\rho\overline{\zeta_o Q} \tag{39}$$

The term on the left-hand side of equation (39) is the mean power associated with the drag and is the focus of this analysis since it contains the power generated by the turbines. Equation (39) states that the power associated with the drag is equal to the rate of work done by the forcing tides at the channel entrance. If equation (37) is substituted into the right-hand side of equation (39), it follows from equation (36) and the orthogonality of the different Fourier modes that

$$g\rho\overline{\zeta_o Q} = g\rho\omega A_b\alpha_1\sin(\phi_1)$$

Therefore, only the first mode in the Fourier series can affect the power, suggesting that keeping only the first mode might be a good approximation.

To further examine this possibility, the full solution to equations (34) and (35) was calculated numerically, and then the Fourier series coefficients of ζ_b were calculated. This was done for the undisturbed state and at maximum turbine power. For comparison, the Fourier coefficients for the simulated Minas Basin tides for the undisturbed and maximum power case were also calculated. The results are shown in

Table 2 The Fourier series coefficients of the solution ζ_b to the theoretical model, (34) and (35), and the simulated Minas Basin tides

	α_1	α_2	α_3	α_4	α_5	α_6
Theory						
Undisturbed	5.053	0.003	0.224	0.003	0.043	0.003
maximum power	3.398	0.001	0.157	0.001	0.041	0.001
Simulation						
Undisturbed	5.302	0.158	0.116	0.003	0.009	0.004
maximum power	3.272	0.064	0.121	0.002	0.020	0.001

Table 2. It is clear that both the theoretical and simulated tides are dominated by the first component, the M_2 tide, and that all the higher harmonics are significantly weaker, less than 5 per cent of the M_2. As well, it is clear that the full theoretical solution is not accurately modelling all the higher modes of the simulated tides. The non-linear interaction in the drag in equation (34) has the form $|Q|Q$ and thus can only excite odd modes, as seen in Table 2. However, in the simulated tides, all higher modes are excited. In particular, in the undisturbed state the second mode, the M_4 tide, has a relatively large amplitude. This suggests that quadratic non-linearities of the form Q^2 are important. Therefore, it can be concluded that using only the first mode in the Fourier series solution (37) is a reasonable approximation.

Based on the above discussion, the solution is assumed to be given by only the first Fourier mode, that is

$$\zeta_b = Ra\cos(\omega t - \phi) \tag{40}$$

and

$$Q = -Ra\omega A_b \sin(\omega t - \phi) \tag{41}$$

where the amplitude of the basin tides is written as a multiple of the forcing amplitude, $R = (\zeta_b)_{max}/a$, ϕ is the phase lag of the basin tides behind the forcing tides and the form of Q follows from equation (35).

Substituting equation (41) into equation (39) gives

$$\lambda^* R^2 = \beta^2 \sin\phi \tag{42}$$

where

$$\lambda^* = \frac{8}{3\pi}\frac{ga}{c^2\omega^2} \quad \beta = \frac{g}{A_b\omega^2 c} \tag{43}$$

Similarly, a second equation can be found by multiplying equation (34) by ζ_b, averaging over a tidal period and integrating the first term by parts to get

$$-c\overline{Q^2} + \lambda\overline{|Q|Q\zeta_b} = g\overline{\zeta_o\zeta_b} - g\overline{\zeta_b^2}$$

which, using equations (40) and (41), reduces to

$$(\beta - 1)R = \beta\cos\phi \tag{44}$$

Finally, equations (42) and (44) can be solved for R and ϕ to give

$$R^2 = \frac{2\beta^2}{(\beta-1)^2 + \sqrt{(\beta-1)^4 + 4(\lambda^*)^2}} \quad \text{and}$$

$$\sin\phi = \frac{\lambda^*}{\beta^2}R^2 \tag{45}$$

APPENDIX 3

Numerical model description

The numerical simulations were run using FVCOM [**15**, **16**]. The grid that was used for the simulation was a refinement of a grid generated by David Greenberg at the Bedford Institute of Oceanography. The original finite-element grid had 9521 triangular elements (Fig. 10) and covered the Bay of Fundy, the Gulf of Maine, and part of the Atlantic Ocean (Fig. 1). To increase the resolution of the grid, each triangular element in the original grid was divided into 16 similar triangles, ensuring that the desirable properties of the original grid were maintained. The final grid has a total of 152 336 non-uniform triangular elements, with 57 684 located in the Bay of Fundy, 1748 in the Minas Passage, and 13 721 in the Minas Basin. The

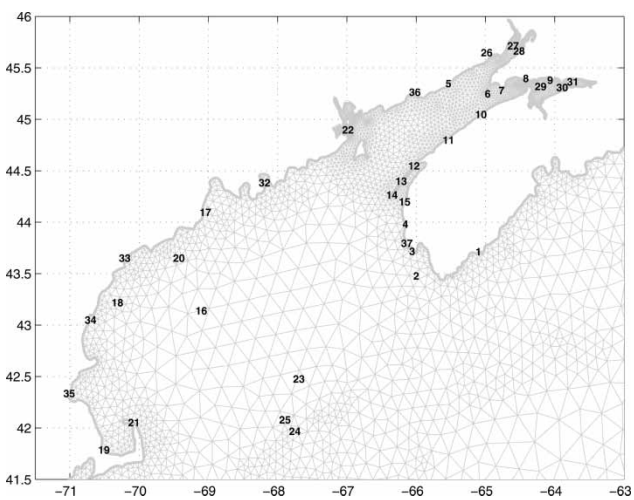

Fig. 10 The figure shows the location of the tidal stations given in Table 3. It also shows some of the grid developed by David Greenberg. The grid that was used for the results presented in this paper has each of these triangular elements divided into 16 similar triangles

Table 3 The amplitudes (m) and phases (°) of the tides from observations and as modelled in the numerical simulations. The final three columns give the difference between the amplitudes and phases and the error (m) given by equation (46). The last row gives the root mean square of the amplitudes, differences, and error. The locations of the stations are shown in Fig. 10. The observed data were provided by David Greenberg of the Bedford Institute of Oceanography

		Observed		Modelled		Difference		
Station	#	Amp.	Phase	Amp.	Phase	Amp.	Phase	Error
Lockport	1	0.70	−1	0.72	−1.6	−0.02	−0.6	0.02
Seal Island	2	1.20	52	1.29	54.0	−0.08	2.0	0.09
Pinkney	3	1.55	59	1.52	61.3	0.03	2.3	0.07
Port Maitland	4	1.85	66	1.86	63.8	−0.01	−2.2	0.07
St Martins	5	3.69	102	3.68	101.1	0.01	−0.9	0.06
Isle Haute	6	4.18	99	4.07	96.5	0.11	−2.5	0.21
Cape D'Or	7	4.34	102	4.28	97.1	0.06	−4.9	0.37
Diligent River	8	4.88	113	4.82	105.6	0.06	−7.4	0.63
Five Islands	9	5.42	125	5.48	122.6	−0.06	−2.4	0.24
Margretsville	10	3.86	93	3.88	89.4	−0.02	−3.6	0.24
Parkers Cove	11	3.43	90	3.36	88.4	0.07	−1.6	0.12
Centreville	12	2.65	90	2.70	94.3	−0.05	4.3	0.21
West Narrows	13	2.23	78	2.44	72.3	−0.21	−5.7	0.32
Westport	14	2.20	80	2.18	79.1	0.02	−0.9	0.04
Meteghan	15	2.03	72	2.07	71.9	−0.04	−0.1	0.04
Cashes Ledge	16	1.20	98	1.24	100.0	−0.04	2.0	0.06
Rockland	17	1.50	98	1.48	100.5	0.02	2.5	0.07
Cape Porpoise	18	1.27	103	1.32	105.1	−0.05	2.1	0.07
Cape Cod Canal	19	1.24	109	1.38	109.5	−0.13	0.5	0.13
Monhegan	20	1.30	99	1.34	101.2	−0.04	2.2	0.06
Cape Cod Lighthouse	21	1.16	113	1.18	115.8	−0.02	2.8	0.06
Eastport	22	2.61	99	2.64	99.6	−0.03	0.6	0.04
B6	23	0.88	87	0.89	88.3	−0.01	1.3	0.02
D/M2	24	0.77	93	0.77	93.5	−0.00	0.5	0.01
M1	25	0.78	92	0.82	91.9	−0.04	−0.1	0.04
Offshore Chignecto	26	4.18	103	4.27	100.4	−0.09	−2.6	0.21
Offshore Grindstone	27	4.82	105	4.65	101.0	0.17	−4.0	0.37
Offshore Cumberland	28	4.74	105	4.67	101.6	0.07	−3.4	0.29
Offshore Minas	29	5.48	121	5.35	117.9	0.13	−3.1	0.32
Offshore Economy	30	5.89	126	5.73	122.3	0.16	−3.7	0.41
Offshore Cobequid	31	6.06	129	5.91	123.3	0.15	−5.7	0.61
Bar Harbor	32	1.55	93	1.57	94.4	−0.02	1.4	0.04
Portland	33	1.33	103	1.36	106.4	−0.03	3.4	0.08
Portsmouth	34	1.30	107	1.33	111.7	−0.03	4.7	0.11
Boston	35	1.34	111	1.36	116.2	−0.02	5.2	0.12
Saint John	36	3.04	98	3.05	97.2	−0.02	−0.8	0.04
Yarmouth	37	1.63	63	1.66	63.1	−0.03	0.1	0.03
r.m.s		3.13		3.10		0.08	3.1	0.23

average area of a triangular element is about 4 km^2; however, the resolution is greater in the Minas Passage and the Minas Basin, where the average areas are 0.043 and 0.079 km^2, respectively. This is a much finer grid than that used in references [**2**] and [**5**] but slightly coarser than the resolution used by reference [**14**], which examined the Bay of Fundy using 75 000 elements.

The M_2 tidal phase and amplitude were specified on the open boundary, and a fixed time step of 1/34 560 of the M_2 tidal period was used. The model was spun up for 12 tidal cycles and the analysis was carried out for the next four tidal cycles. The minimum bottom friction was tuned to give the lowest error as calculated using the following formula from reference [**14**]

$$\text{Error} = \left|A_{\mathrm{m}}\mathrm{e}^{i\theta_{\mathrm{m}}} - A_{\mathrm{c}}\mathrm{e}^{i\theta_{\mathrm{c}}}\right| \tag{46}$$

where A_{m} and A_{c} are the measured and calculated tidal amplitude in metres and θ_{m} and θ_{c} are the measured and calculated tidal phases in radians, respectively. This bottom-friction coefficient was 0.0026. In comparison, reference [**14**] used a coefficient of 0.0025, whereas reference [**5**] used 0.002. To achieve accurate results, reference [**2**] used two different values: 0.0024 in the Gulf of Maine and 0.0021 for the remainder of the region.

The phase and amplitude of the tidal elevation were calculated at each node and are compared with observations in Table 3. The root mean square of the difference in amplitude, the difference in phase, and the error are 8 cm, 3.1°, and 23 cm, respectively. These are similar to previous results [**5, 14**].

Copyright of Proceedings of the Institution of Mechanical Engineers -- Part A -- Power & Energy is the property of Professional Engineering Publishing and its content may not be copied or emailed to multiple sites or posted to a listserv without the copyright holder's express written permission. However, users may print, download, or email articles for individual use.